Proc Indian Natn Sci Acad, **70, A,** No. 2, March 2004, pp. 367-382

A BIO-INSPIRED APPROACH FOR CONTROLLING THE PRIMARY AND SECONDARY COORDINATION SPHERES OF METAL IONS CONFINED WITHIN POROUS MATERIALS

A S BOROVIK

Department of Chemistry, University of Kansas, Lawrence, KS 66045 (USA)

(Received 24 January 2003 ; Accepted 06 February 2003)

Development of materials whose function is correlated to the structure of immobilized active sites is one of the challenges in material science. The structures of metalloproteins offer some guides into incorporating inorganic species within porous organic hosts. We have employed a "molecules to materials" methodology, which relies on the design and synthesis of well-defined monomeric species. Copolymerization with organic crosslinkers affords functional, porous materials whose properties differ from analogous complexes in solutions. This review describes the details of the design process, synthesis of the monomeric templates, methods of material fabrication, and techniques used to probe the structure and function of metal active sites dispersed within new porous materials.

Key Words: Coordination Compounds; Bioinorganic Chemistry; Reversible Dioxygen Binding; Porous Polymers; Cobalt Complexes; Template Copolymerization.

Introduction

The design and synthesis of metal complexes has advanced significantly in the last 50 years. We are at a stage in the development of inorganic species where the placement of nearly any donor group around metal ions is possible. This has lead to better control of the primary coordination sphere around metal ions, which enables the regulation of various functional properties, such as the stereochemistry, electronic structure, redox processes and Lewis acidity. Progress has also been made in the design and construction of structures that do not directly bind to metal ions but can influence the secondary coordination sphere, which is important in controlling reactivity. Most of these advances have occurred within the realm of low-molecular weight metal complexes, that is those systems which readily dissolve in a solvent. These complexes often have lengths on the order of 1-5 nm.

Increasing the size (i.e. length) of metal complexes is one of the challenges inorganic chemists face at the dawn of the new millennium. An increase in the length range of complexes is advantageous for applications where multi-metal centres are necessary for function. In addition, there is the need to develop heterogeneous systems, which often require an increase in the length scale of the metal complex. Since function is closely coupled to structure in these systems, precise control of the primary and secondary coordination spheres has to be maintained during this "scaling up" process. However, it has proven difficult to control the molecular architectures around metal ions when the length scale of the complex has been increased above 5 nm.

One approach to solving this length scale problem is to design and prepare monomeric precursors, which can be assembled into larger functional units. These monomers can be studied in solution by conventional techniques and subsequently incorporated into larger arrays to yield new functional entities. Many of these systems are in the crystalline phase and have produced exciting systems for gas binding/storage and materials with new physical properties. Examples of these types of systems include those of Lehn[1], Yaghi[2], and Long[3].

We have chosen a complementary approach to other researchers, utilizing immobilization of metal complexes within porous organic materials. This approach uses monomeric organic and inorganic precursors, which are polymerized under radical conditions to yield porous materials. Although the porous host is an amorphous solid, the structure of the immobilized sites can be fixed during the copolymerization and maintained after the process has been completed. We have tested and verified these ideas and found that new chemical properties arise from the confinement of metal complexes within porous hosts. A summary of the design, synthesis and properties of several new porous materials will be the subject of this review[4].

Genesis of the Design

Metalloproteins have functions that have yet to be mimicked in synthetic systems. A major cause for this is that metalloproteins have evolved specific architectural features within their active sites, which are essential for function. Synthetic methods have not advanced to the point where duplications of all these architectural properties is possible. For example, one of the most important of properties for metalloproteins is the site isolation capacity of the protein matrix. In many instances, metalloactive sites are located within the interior of the protein. This isolation of the active site by the organic protein matrix prevents the metal centres from undergoing undesirable metal-metal interactions. Site isolation also aids in regulating coordination to the metal centre(s), which often have to be coordinatively unsaturated to be active, and in controlling the secondary coordination sphere (microenvironment) of the metal complex.

This control of the microenvironment is strongly coupled to the function of most metalloproteins. Biophysical studies on a variety of different proteins have revealed that essential properties for protein function (*e.g.*, hydrophobicity, allostery, and electrostatic effects) are managed by the molecular structures of the metal active sites. The chemical microenvironments found in the protein active sites result from the placement of functional groups at precise locations. This positioning produces active site structures having shape and chemical characteristics that ensure selective binding of exogenous ligands (including substrates) and regulation of subsequent chemistry. The effects of site isolation and microenvironmental control on the function of metal ions in proteins are clearly illustrated by the diverse activity of heme-containing proteins. In hemoglobin and myoglobin, the steric constraints and hydrogen bond capacity of the distal site of the isolated heme pockets (Fig. 1) has a dramatic impact on the dioxygen binding properties of these proteins[5]. Altering the position of the distal histidine has pronounced functional effects, an example of which is the enhanced peroxidase activity observed for myoglobins whose active sites have been engineered to eliminate bifurcated H-bond formation[6]. In oxygenases and peroxidases, the functions of the enzymes are affected greatly by the various protein environments that house the catalytic iron heme moieties. For instance, cytochrome P_{450} (a monooxygenase) and chloroperoxidase (which halogenates substrates) have identical heme active site with axially bonded thiolates, yet the functions are vastly different[7]. This activity difference has been attributed to differences in the microenvironments around the active iron heme units.

While confined within the framework of the protein host, metalloprotein active sites are accessible to external ligands (or substrates) through channels or clefts that connect that active site to the molecular surface of the protein. Recent molecular structures of metalloproteins illustrate how various proteins use site isolation and channels to help regulate chemical transformations. Lipoxygenase is an example of such a protein[8]. This non-heme iron enzyme catalyzes the dioxygenation of arachidonic acid with O_2 and has two channels that connect the isolated active site to the exterior of the protein. One channel is postulated to provide O_2 to the iron centre, whereas the second channel appears to be designed to accommodate the arachidonic acid substrate.

Design Considerations for Confining Metal Complexes in Porous Hosts

We sought to establish a general synthetic methodology to prepare materials that utilized aspects of molecular architecture found in metalloproteins. The approach developed is interdisciplinary, in that it combines inorganic and organic chemistry with material science to confide metal complexes within porous organic hosts. The polymeric organic hosts are designed to model several properties of protein-derived structures, including the capacity to site isolate metal complexes, while ensuring access of external molecules to the

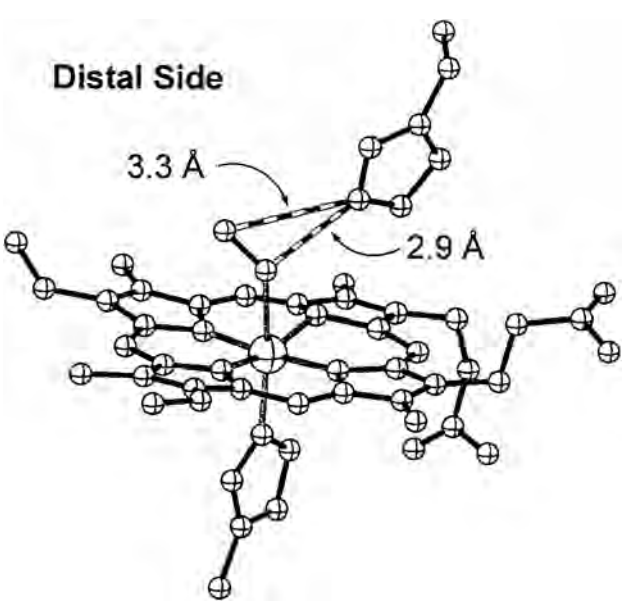

Fig. 1 The active site of oxymyoglobin emphasizing the distal H-bonds. H atoms not shown.

immobilized complexes by a porous network structure. Moreover, the immobilized metal site structure can be controlled, allowing for the potential regulation of the microenvironment around the functional centres. A comparison between our systems and those of hemoglobin are presented in Fig. 2.

We have used template copolymerization methods to prepare our systems, which is often used to make imprinted polymers[9,10]. Formation of the immobilized metal sites occurs during polymerization, allowing each site to have the same morphology and arrangement of ligands (or functional groups) as the template compound. The hosts are not polypeptides, but rather, highly crosslinked organic polymers, which are made from organic monomers containing activated vinyl groups. A large excess of organic monomer is used to afford highly crosslinked organic polymers with permanent porous structure. The high crosslinking (>90%) ensures the porous structure while providing hosts that are sufficiently rigid to maintain the structure of the immobilized sites. Although the hosts themselves are amorphous, the structure of the immobilized sites within the hosts, in theory, should be well-defined and can be tailored to a desired function by using templates that are formed prior to polymerization. Thus we are using molecular species, whose properties are determined before material growth, to construct the porous hosts and the immobilized sites where function will occur.

This methodology should produce systems that are able to overcome two longstanding problems that have plagued this area of materials science: access to the immobilized sites and maintenance of the desired stereochemistry of the metal complexes in the solid state. In porous materials made by other methods, limited accessibility to the immobilized site is often hampered because of the instability of the porous structure. The permanent pores within our materials are able to connect a high percentage of immobilized sites (up to 90%) to the polymeric surface. This allows continuous access of external species to the immobilized metal complex, which is usually necessary for function.

The structure of the immobilized sites is essential for regulating functional properties, yet this is difficult to control after confinement has occurred (vide supra). Because function is correlated to the precise spatial arrangement of ligands within the immobilized sites, it is necessary to define the primary and secondary coordination spheres around the metal ion(s). The inability to place essential ligands in the correct locations with the immobilized sites often leads to dysfunction. The use of template copolymerization methods has allowed us to manipulate the small length scales (0.5-1 nm) of the metal complexes confined to the immobilized site, even though the overall length of the materials are greater than 1 μm.

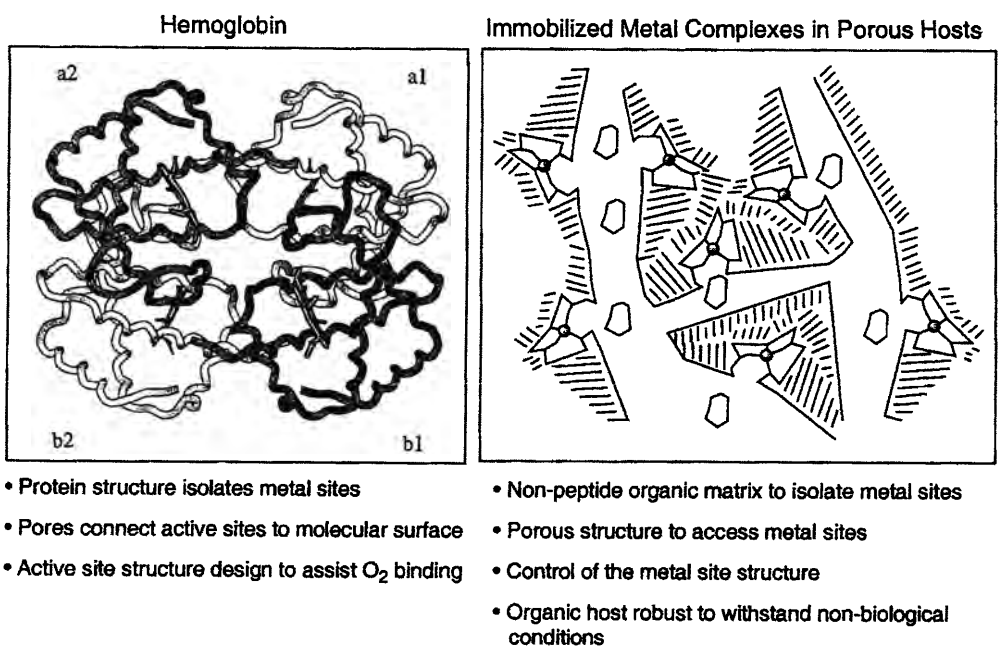

Fig. 2 Structural comparison of human hemoglobin to the designed synthetic materials

Description of the Copolymerization Methodology

The general synthetic protocol is outlined in Scheme 1. Template metal complexes are assembled in solution prior to polymerization; this is advantageous because greater control of the immobilized site structure is achieved using templates of known molecular structure and the amount of species incorporated into the porous host can be carefully regulated. Note that the ligands have activated vinyl groups, which eventually will be covalently connected to the polymer host. We employ template complexes that are substitutionally inert because they can be structurally characterized before immobilization, so we can ensure that all the ligands are bonded to the metal centre(s). This aids in regulating the relative disposition of the ligands within the immobilized sites. Once assembled and characterized, the template complex is combined with a large excess of crosslinking agent (greater than 90 mole percent) and the mixture is dissolved in a suitable solvent. This homogeneous solution is polymerized using either heat or light to afford an insoluble monolith. During growth of the network polymer, the template complexes are covalently linked to the organic backbone through the vinyl groups on the ligands. Thus immobilized sites are formed, which have size and shape characteristics of the template. In addition, the solvent acts as a porogen to form the channels that run throughout the material. After polymerization is completed (usually 24-48 h), the polymeric monolith is broken apart by grinding, subjected to continuous extraction, dried, and sieved to a uniformed particle size. We have worked with particles that are less than 120 μm.

In our scheme, two general options are available once the materials are prepared and purified. Chemical processes can immediately be studied for coordinatively unsaturated immobilized complexes because the species have accessible binding sites. The second option involves removal of the template metal ion to produce sites with new chelating ligands whose microenvironment is controlled by the porous host. The donor atoms of the chelates (indicated in Scheme 1 by the geometrical shapes) remain in the immobilized sites because they are covalently attached to the host during the copolymerization process. Rebinding of metal ions to the immobilized sites allows us to synthesize new metal complexes whose properties can be different from those derived from solution.

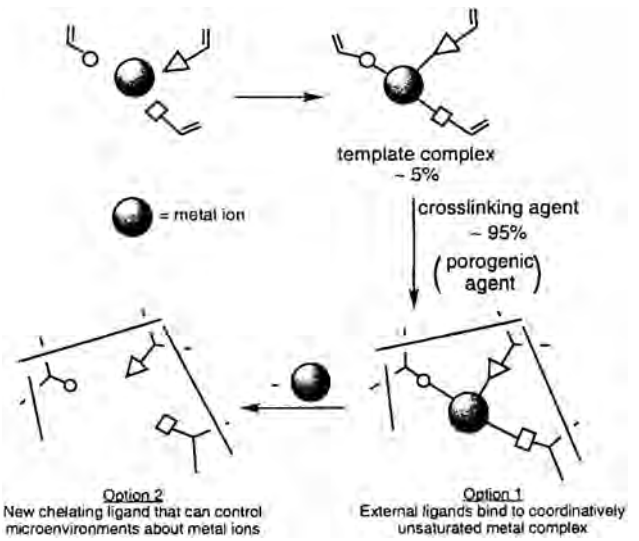

Scheme 1

Comparison of the Approach to Other Methodologies

Since Merrifield's seminal work on the use of solid supports in peptide synthesis[11], many systems have been reported that use solid supports to develop metal-based catalyst and synthetic reagents[12]. The most common synthetic approach is the attachment of catalysts to preexisting solid supports. Often these are synthesized by chemically modifying linear or partially crosslinked (2-20%) polymers[13-15] or non-covalent inclusion of the catalysts into porous hosts, such as zeolites[16] or membranes[17]. Varying degrees of success have been found for these synthetic routes. Attachment of catalysts to preformed polymers is limited to their surfaces, which hinders the regulation of the catalytic centres. Also, the low amount of crosslinking in these solids produces relatively flexible supports, which does not prevent metal-metal interactions that are often required in oxidation catalysts. Zeolites have cages whose size and shape are fixed prior to inclusion of the metal catalysts. This inability to tune the structure of the catalytic sites limits control of the active site structure. In addition, leaching of the catalysts from the support can occur because inclusion occurs by non-covalent interactions[18].

The synthetic approach we use is fundamentally different from the ones described above. The immobilized sites formed in our systems are constructed from their monomeric components by copolymerizing templates with a large excess of organic crosslinking agent. The resulting compounds are sufficiently rigid to retain the metal site architecture generated during

polymerization while preventing unwanted metal-metal interactions. The porosity of the organic hosts allows solvent and potential substrates access to nearly all the immobilized metal complexes that are dispersed throughout the host. Moreover, leaching of the metal complexes is blocked because the ligands within the immobilized sites are covalently bonded to the porous hosts.

Development of a Structural Probe for the Immobilized Sites

Our early systems established that diatomic gases, such as CO, reversibly bind to metal complexes immobilized in porous organic hosts. In addition, the hosts were able to confine the metal complexes so that intermolecular interactions were limited[4a,b]. However, these initial systems did not address aspects of the architecture of the immobilized sites; in particular, those involving the primary and secondary coordination spheres of the metal ions. In fact, little is known about the immobilized site structure in materials made by template copolymerization. The vast majority of materials made by this methodology have used organic-based templates. Direct examination of the immobilized site structures is difficult for organic-based templates because there are a few tools that can distinguish the key components of the immobilized sites from those of the host, which are present in such large excess. In these organic based systems, site structure is often inferred from batch rebinding studies. Thus key structural factors have not been addressed, including whether the relative spatial dispositions of functional groups within the immobilized sites are maintained after removal of the template[19]. We anticipated that the immobilization of metal complexes within porous organic hosts would provide a means to probe these structural issues. The diverse spectroscopic properties of metal complexes allow investigations into the site structure within organic hosts. For our studies, we have used X-ray absorption and electron paramagnetic spectroscopies (XAS and EPR, respectively) to probe site structure.

The probe system developed to examine the structure of immobilized metal complexes is based on the chemistry of [Co(II)(salen)O_2] (Scheme 2)[20] . In solution, the four-coordinate [Co(II)(salen)] weakly binds dioxygen. In contrast, the five-coordinate square-pyramidal [Co(II)(salen)(py)] complex, has a relatively large affinity for dioxygen. This change in dioxygen affinity has been rationalized on electronic grounds

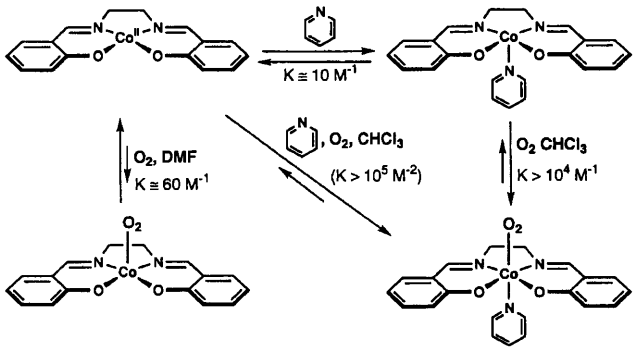

Scheme 2[19]

because in [Co(II)(salen)(py)] the energy of the d_{z^2} orbital is raised above that of the d_{xy} orbital to give a $(d_{xz})^2(d_{yz})^2(d_{xy})^2(d_{z2})^1$ configuration[21]. Note that [Co(II)(salen)] complex weakly binds pyridine under anaerobic conditions ($K_a \sim 10\ M^{-1}$) but in the presence of dioxygen forms the tertiary [Co(II)(salen)(py)(O_2)] complex with an estimated binding constant of 10^5.

These [Co(salen)] complexes are useful probes for the site structures in porous hosts because each species has different EPR properties. Although the three principal complexes, [Co(II)(salen)], [Co(II)(salen)(py)], and [Co(salen)(py)(O_2)], have $S = 1/2$ ground states, they have distinguishable EPR spectra. These differences in spectral properties allow for the direct examination of the coordination geometry around the Co(II) ion within the immobilized site. Thus we can evaluate the placement and binding of weakly coordinating endogenous ligands (pyridine) to immobilized [Co(II)salen] complexes and examine their interactions with external ligands, such as dioxygen.

Our synthetic approach, shown schematically in Fig. 3, involves preparing materials with immobilized sites having the correct arrangement of ligands to support square pyramidal coordination geometry about Co(II) ions. The site structure is formed utilizing a substitutionally inert, *six-coordinate Co(III) complex*. We have found that the use of inert metal complexes as templates produces materials with homogeneous sites; that is, the immobilized sites have similar architecture. Using Co(III) complexes assure that the ligands will remain in place during polymerization (vide infra). Three-point binding of the template within the immobilized site was envisioned—two are in the equatorial plane from the salen ligand and one in the axial position arising from a monodentate ligand. The final coordination site on the template complex is taken

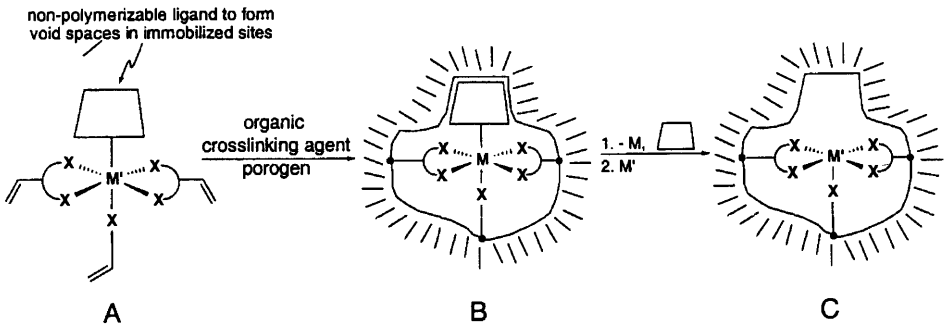

Fig. 3 Schematic depicting the template copolymerization method used for synthesizing coordinatively unsaturated metal sites immobilized in porous organic hosts. Substitutionally inert template complexes used to form the immobilized sites (**A**); immobilized sites after polymerization showing the spatial arrangement of ligands around the metal (**B**); and modified immobilized sites containing metal complexes with vacant coordination sites (**C**).

by a nonpolymerizable ligand whose only connection to the polymer is through its bond to the metal centre. After polymer formation, the cobalt ion and the nonpolymerizable ligand are removed from each site by chemical methods. The immobilized sites will then contain endogenous ligands that are disposed to rebind a Co(II) ion and form a square-pyramidal complex. This design has allowed us to probe the binding of an endogenous pyridine ligand to immobilized [Co(II)(salen)] complexes.

We reasoned that if ligands within the site were rigidly fixed, as implied by the cartoon in Scheme 1, then a large proportion of five-coordinate sites would be observed. However, if the Co(II) complexes within the sites were relatively flexible, they would have properties like those in solution (Scheme 2) and a distribution of sites containing four- and five-coordinate complexes would be expected. EPR spectroscopy can be employed to study the coordination geometry of the immobilized Co(II) centres and we can obtain information about the flexibility of the ligands within the immobilized sites.

In order to bind dioxygen, the immobilized sites produced from this approach must stabilize coordinatively unsaturated cobalt complexes within the hosts. The formation of coordinatively unsaturated complexes has been one of the recent challenges in material science. In our systems, the template complex contains a nonpolymerizable ligand, which serves to carve out void space around each metal centre, and is removed from the immobilized sites during demetallation. This allows other ligands, not present during polymerization, to bind to the immobilized sites. Moreover, the porous host sufficiently isolates the immobilized sites to prevent unwanted metal—metal

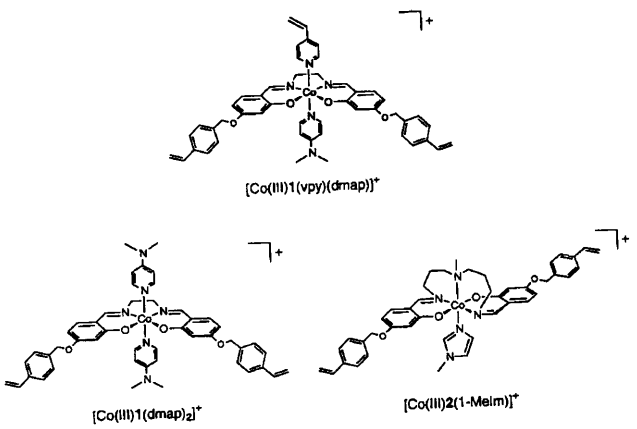

Fig. 4 Template complexes used to make the immobilized metal sites in porous organic hosts.

interactions that lead to irreversible dioxygen binding, which is often found for [Co(II)(salen)] complexes in solution.

Template Complexes[4c-g]

Fig. 4 shows the Co(III) complexes used as template. [Co(III)**1**(vpy)(dmap)]$^+$ was utilized to form immobilized sites containing five endogenous donors to the cobalt centre. This complex has necessary features needed to make the proposed sites, including (1) three appended vinyl groups that provide three-point binding, two from the bis[2-hydroxy-4-(4-vinylbenzyloxy)benzaldehyde]ethylenediimine (H_2**1**) and one from 4-vinyl-pyridine (vpy); and (2) an axially coordinated (4-dimethylamino)pyridine (dmap), a nonpolymerizable ligand, which creates void space for eventually binding of dioxygen.

A second complex, [Co(III)**1**$(dmap)_2]^+$, was used to make a porous material which contains immobilized sites with just the salen ligand covalently attached.

Dmap ligands are axially coordinated to the Co(III) centres in these complexes and are removed after polymerization is completed. Rebinding of Co(II) ions renders the sites as four-coordinate, square-planar [Co(II)salen] complexes. Thus this material serves as a control to assess the importance of placing an endogenous pyridine ligand perpendicular to the equatorial plane. The final template complex is $[Co^{III}\mathbf{2}(1\text{-MeIm})]^+$, which contains the pentadentate ligand $[\mathbf{2}]^{2-}$, bis[2-hydroxo-4-(4-vinylbenzyl-methoxy)-benzyliminotapropyl]methylamine. This ligand has the advantage of incorporating a tertiary amine nitrogen donor that binds to the metal ion at one of its axial coordination sites. Similar to the role of the dmap ligand in the previous two templates, 1-MeIm serves to create void space in the confined sites and is removed after polymerization. Note that $[Co(III)\mathbf{1}(vpy)(dmap)]^+$, $[Co(III)\mathbf{1}(dmap)_2]^+$, and $[Co^{III}\mathbf{2}(1\text{-MeIm})]^+$ are diamagnetic and substitutionally inert under the conditions of polymerization. The assignment of the structures for these template complexes in solution is supported by their ^1H NMR spectral properties, examples of which are shown in Fig. 5 for $[Co(III)\mathbf{1}(vpy)(dmap)]^+$ and $[Co(III)\mathbf{1}(dmap)_2]^+$.

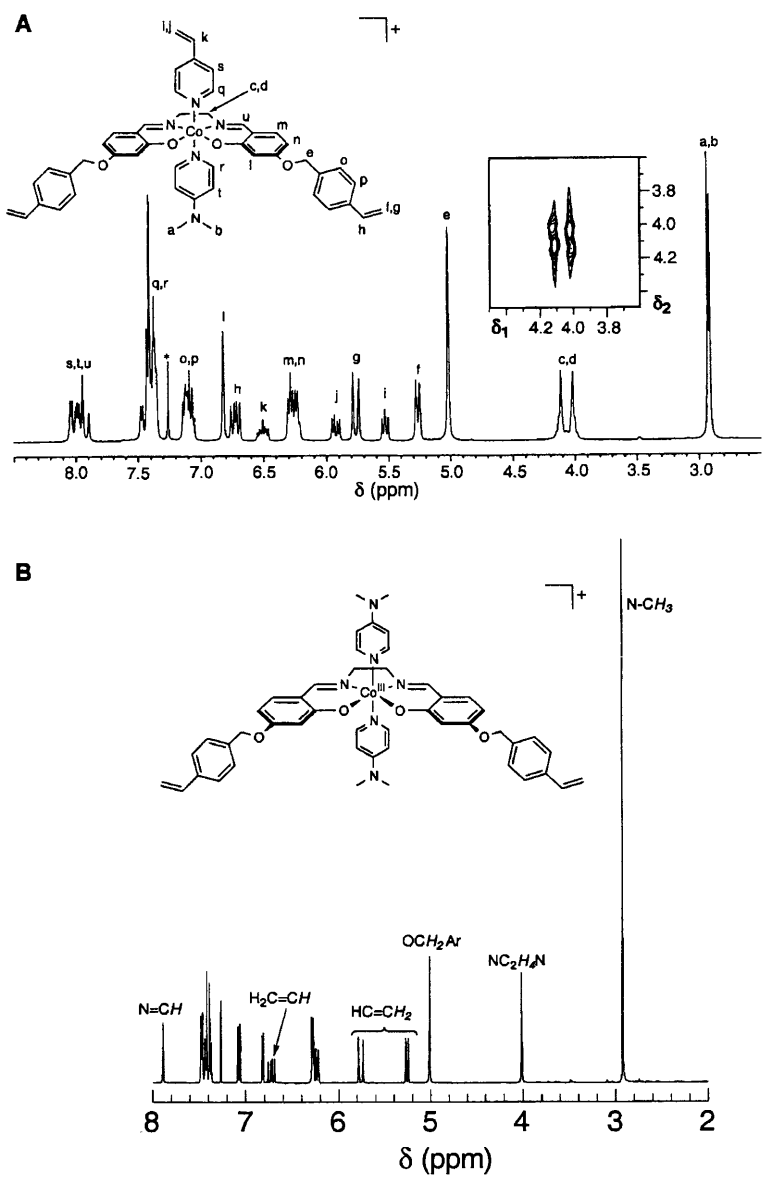

Fig. 5 400 MHz ^1H NMR spectrum of the template complex $[Co(III)\mathbf{1}(vpy)(dmap)]PF_6$ (**A**) and $[Co(III)\mathbf{1}(dmap)_2]PF_6$ (**B**). Inset in **A** contains a portion of the ^1H NMR COSY spectrum of the complex, showing the cross peaks for the diastereotopic protons on the ethylene backbone of **1**.

Polymerization Process

Scheme 3 illustrates the synthesis for immobilizing [Co(III)**1**(vpy)(dmap)]PF_4 within a polymethacrylate host[4d]. A 5%:94% mole ratio of [Co(III)**1**(vpy)(dmap)]PF_4 to crosslinker (ethylene glycol dimethylacrylate, EGDMA) was employed with nitromethane acting as the porogen. After polymerization was completed, the monolithic polymer, P-**1**·**py**[Co(III)(dmap)] was crushed, continuously extracted for 24 h, and sieved to achieve particles of <125 μm, which contained an average of 180 μmol Co/g of polymer. In order to reversibly bind dioxygen, the complexes within the immobilized sites needed to be converted to five-coordinate Co(II) complexes; this was accomplished using a three-step chemical procedure. The Co(III) centres in P-**1**·**py** [Co(III)(dmap)] were reduced with $S_2O_4^{2-}$ and the cobalt ions were removed with $[EDTA]^{2-}$. This process removed approximately 90% of the dmap ligands and cobalt ions from the polymer. The resultant apo polymer (P-**1**·**py**) readily rebinds Co(II) ions to afford P-**1**·**py**[Co(II)].

The preparation of the control polymer, P-**1**[Co(II)] is outlined in Scheme 4[4c,g]. The monomers [Co(III)**1**$(dmap)_2$]PF_4 and EGDMA were copolymerized in DMF using identical conditions as described above. The nearly quantitative (> 90 %) removal of Co(III) ions and the dmap ligands was achieved by refluxing P-[Co(III)**1**$(dmap)_2$] in an aqueous solution of 0.1 M Na_2EDTA at a pH < 4. These conditions also hydrolyzed the immobilized salen ligand to yield sites composed of two salicylaldehyde moieties covalently attached to the organic host (P-**1**·$(\mathbf{sal})_2$). The predisposition of these aldehydes within the sites allows for regeneration of the salen ligand by treating P-**1** $(\mathbf{sal})_2$ with ethylenediamine. This produces P-**1**, which readily binds Co(II) to afford P-**1**[Co(II)], and has immobilized sites with four-coordinate Co(II) complexes. The hydrolysis route (Scheme 4) was also used to prepare P-**2**[Co(II)], with the triamine, 3,3'-diamino-*N*-methyldipropylamine being used to reform the **2** within polymeric sites.

Based on porosity measurements, P-**1**·**py**[Co(II)], P-**1**[Co(II)] and P-**2**[Co(II)] are mesoporous materials with average pore diameters of 20-60 Å. Similar porosity values were found for the starting polymers having Co(III) centres within the immobilized sites, indicating that the pores are unaffected by chemical modification.

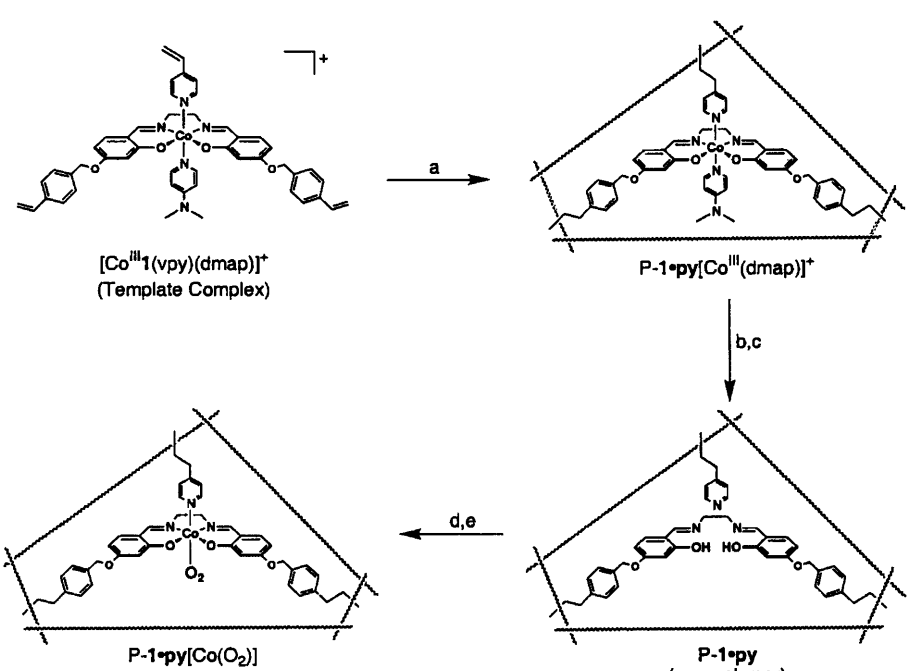

Conditions: (a) EGDMA, AIBN, CH_3NO_2, Ar, 60°C, 25 h; (b) $Na_2S_2O_4$, MeOH, Ar, 2h; (c) $(NMe_4)_2EDTA$, MeOH, Ar, 6 h; (e) O_2, CH_3NO_2.

Scheme 3

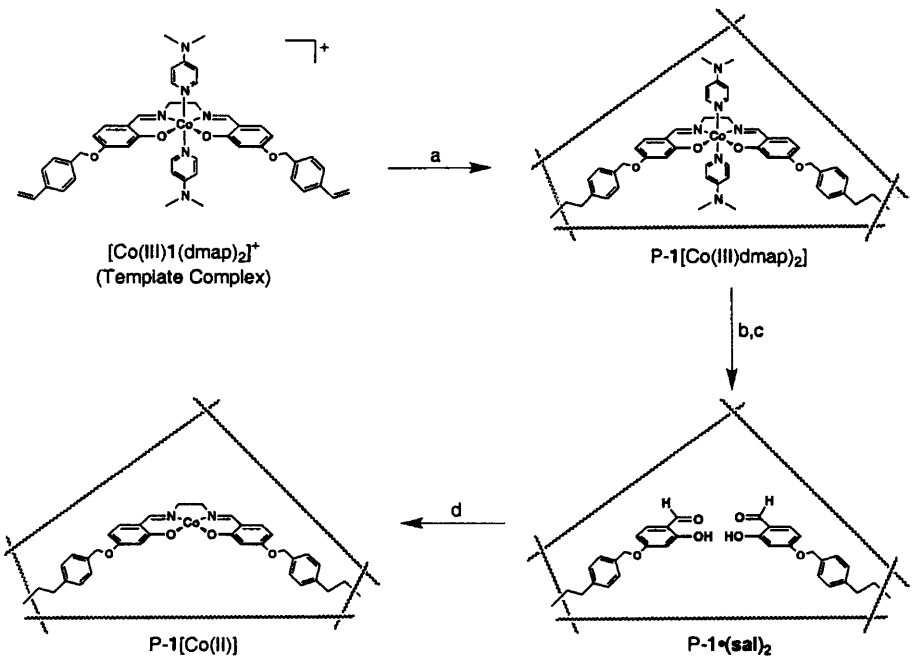

Conditions: a, EGDMA, AIBN, DMF, N_2, 60°C; b. EDTA, H_2O, Δ; c, $C_2H_8N_2$, MeOH; d, $Co(OA)_2$, MeOH, N_2

Scheme 4

Probing the Fate of the Template Complexes after Copolymerization[4g]

Our approach relies on the Co(III) template complexes maintaining their structures during copolymerization. To probe this issue, X-ray absorption spectroscopy was used to analyze the structural properties of the immobilized sites in P-**1**[Co(III)(dmap)$_2$] and P-**2**[Co(III)(1-MeIm)]. We took advantage of the result that both [Co(III)**1**(dmap)$_2$]PF_4 and [Co(III)**2**(1-MeIm)]PF_6 readily crystallized and their crystal structures could be analyzed by single crystal X-ray diffraction techniques. We thus used these crystallographic data on the monomeric [Co(III)**1**(dmap)$_2$]$^+$ and [Co(III)**2**(1-MeIm)]$^+$ complexes to verify the XAS results obtained on the Co(III) monomers and polymeric species.

X-Ray Diffraction Studies on the Template Complexes

The molecular structures of [Co(III)**1**(dmap)$_2$]$^+$ and [Co(III)(1-MeIm)]$^+$ are shown in Fig. 6. Both are six-coordinate, with the expected arrangement of ligands around the Co(III) ions. The bond distances for the primary coordination spheres are given in Table I. For both complexes, the 4-vinylbenzyloxy groups, which are needed for polymerization, are extended outward

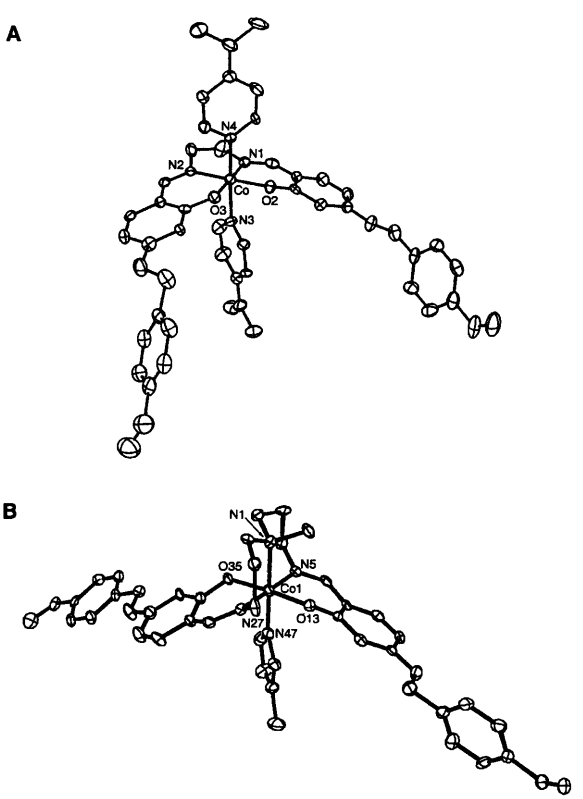

Fig. 6 Thermal ellipsoid diagrams of [Co(III)**1**(dmap)$_2$]$^+$ (**A**) and [Co(III)**2**(1-MeIm)]$^+$ (**B**). The ellipsoids are drawn at the 50% probability level and hydrogens have been removed for clarity.

Table I

Selected Bond Distances and Angles for [Co(III)1(dmap)$_2$]$^+$ and [Co(III)2(1-MeIm)]$^+$

[Co(III)**1**(dmap)$_2$]$^+$	Bond Lengths (Å)	[Co(III)**2**(1-MeIm)]$^+$	Bond Lengths (Å)
Co—N1	1.874(7)	Co—O13	1.888(3)
Co—N2	1.891(7)	Co—O35	1.895(3)
Co—N4	1.961(7)	Co—N47	1.932(4)
Co—O3	1.885(6)	Co—N5	1.936(4)
Co—O2	1.893(5)	Co—N27	1.931(4)
Co—N3	1.997(8)	Co—N1	2.031(5)

from the metal centre and cause no apparent distortion of the primary coordination sphere about the Co(III) ion.

XANES Results for Templates and Co(III) Polymers

Fig. 7 contains the results obtained from X-ray absorption near edge spectra (XANES) for the monomeric template complexes, [Co(III)**1**(dmap)$_2$]$^+$ and [Co(III)**2**(1-MeIm)]$^+$ and the polymers P-**1**[Co(III)(dmap)$_2$] and P-**2**[Co(III)(1-MeIm)]. A pre-edge peak at 7711 eV, which is assigned to a 1s→3d transition, is found in the XANES of [Co(III)**1**(dmap)$_2$]$^+$ and [Co(III)**2**(1-MeIm)]$^+$. The relatively small size of this peak (2-3% of the edge height with an area of 0.05 eV × edge height) is similar to that of six-coordinate synthetic complexes. This feature and its small size are indicative of transition metal complexes having centrosymmetric (octahedral or square planar) coordination geometry. A shoulder at ~7719 eV is also found from our fitting procedure and is assigned to the 1s→4p transition.

Fig. 7 also shows that the XANES data for P-**1**[Co(III)(dmap)$_2$] and P-**2**[Co(III)(1-MeIm)] are virtually indistinguishable from the spectra of their monomeric precursors, [Co(III)**1**(dmap)$_2$]$^+$ and [Co(III)**2**(1-MeIm)]$^+$. The minor differences observed between the two spectra of the monomer complexes are also present in spectra of the corresponding polymer samples. For instances, features near the top of the edge in the XANES region are shifted ca. 2 eV lower in energy for [Co(III)**2**(1-MeIm)]$^+$ and P-**2**[Co(III)(1-MeIm)] compared to P-**1**[Co(III)(dmap)$_2$]. Other small differences are attributed to different hardware used to collect the data. Taken together, these data clearly show that the template complexes retain their molecular structures within immobilized sites

EXAFS Results for Templates and Co(III) Polymers

The analysis of the extended X-ray absorption fine structure (EXAFS) region for these systems further

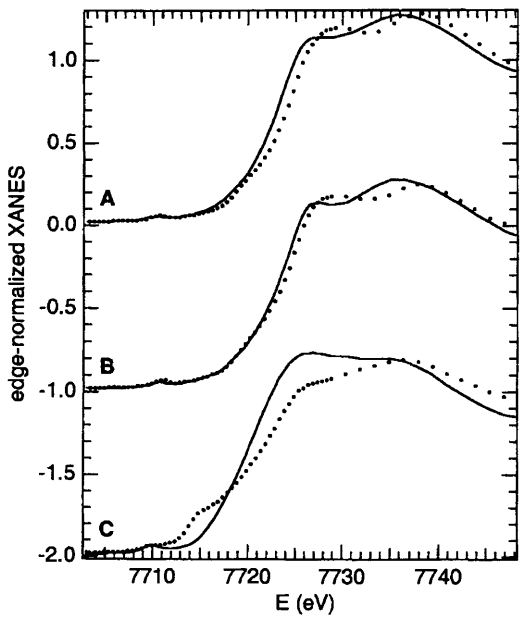

Fig. 7 Edge spectra. For each comparison, XAS of a complex derived from ligand **1** (····) is compared with XAS of a complex derived from ligand **2** (—). (**A**) Monomer ternary complexes [Co(III)**1**(dmap)$_2$]$^+$ and [Co(III)**2**(1-MeIm)]$^+$; offset = 0. (**B**) Polymer ternary complexes P-**1**[Co(III)(dmap)$_2$]$^+$ and P-**2**[Co(III)(1-MeIm)]$^+$; offset = -1. (**C**) Polymer Co^{II} complexes P-**1**[Co(II)] and P-**2**[Co(II)]; offset = -2.

supports the retention of structure for the template complexes when confined within the polymers. EXAFS data of both [Co(III)**1**(dmap)$_2$]$^+$ and [Co(III)**2**(1-MeIm)]$^+$ can be fit well with a two shell model using approximately six nitrogen and/or oxygen atoms at ~1.9 Å and approximately 10 carbon atoms at ~2.8 Å. These data are found in Table II, which includes in italics the values expected for *n* and *r* for the first (Co-N/O) and second (two bond Co-C) coordination spheres based on the structures of the monomers obtained by X-ray diffraction. There is strong agreement between these two structural measurements, showing that the XAS technique can be utilized to probe the structures of our immobilized complexes.

Examination of Table II shows that the refined EXAFS values of the polymers and monomer samples

Table II

Refined Parameters and Uncertainty Ranges for Weighted[a] Fits of Fourier Filtered[b] $k^3\chi$ (FF $k^3\chi$ fits). Crystallographic Data in Parentheses When Available.[c]

	N/O Shell[d]		C Shell[d]				
Sample	n	r (Å)	n	r (Å)	σ (Å)[e]	ΔE_0 (eV)[f]	ε_v^{2g}
$[Co^{III}\mathbf{1}(dmap)_2]^+$	5.6 ± 0.5[h] (6)	1.897 ± 0.007 (1.917)	10 ± 2 (10)	2.84 ± 0.02 (2.87)	0.055 ± 0.009	0.6 ± 1.1	2.8
$[Co^{III}\mathbf{2}(1\text{-MeIm})^+$	5.5 ± 0.6 (6)	1.914 ± 0.008 (1.935)	11 ± 2 (11)	2.87 ± 0.02 (2.902)	0.061 ± 0.009	0.0 ± 1.2	1.3
P-**1**$[Co^{III}(dmap)_2]$	5.3 ± 0.5	1.898 ± 0.007	9 ± 2	2.82 ± 0.02	0.053 ± 0.009	0.3 ± 1.2	8.1
P-**2**$[Co^{III}(1\text{-MeIm})]$	5.5 ± 0.6	1.913 ± 0.007	10 ± 2	2.86 ± 0.02	0.058 ± 0.009	-0.1 ± 1.2	1.8
P-**1**$[Co^{II}]$	3.4 ± 0.5	1.859 ± 0.011	6 ± 2	2.80 ± 0.03	0.054 ± 0.015	-2.0 ± 2.0	0.5
P-**2**$[Co^{II}]$	4.8 ± 0.9	1.962 ± 0.016	9 ± 3	2.91 ± 0.04	0.090 ± 0.015	-2.3 ± 2.3	0.5

[a] Esd_{FF} is interpolated from the following (k Å, esd_{FF} Å^3): (2.2, 0.14), (4, 0.19), (8, 0.26), (10, 0.42), (13, 0.88), (14.3, 0.56). [b] Fourier filtered $k^3\chi$ and $k^3\chi_{sim}$ are denoted FF and FF_{sim}, respectively. F.T.: k = 1.0 to 14.3 Å^{-1} using 5% windowing.[13] Back-transform: r' = 0.90 to 2.45 Å. [c] Average bond lengths and two-bond Co-C distances from crystal structures. [d] EXAFS from each shell ($\chi_{sim} = \chi_1 + \chi_2$) is modelled as $\chi_i = S_0^2 n_i f_i \exp(-2k_i^2\sigma_i^2) \times k_i^{-1} r^2 \sin(2k_i r_i + \alpha_i)$. [e] σ_2 was constrained equal to σ_1. Without this constraint, σ_2 refined to less σ_1, which is unrealistic. [f] The k_i used in calculating χ_{sim} is $k_i = [2 m_e \hbar^{-2} (E - (7723 \text{ eV} + \Delta E_0))]^{0.5}$. [g] The minimized residual, $\varepsilon_v^2 = [n_{idp}/(n_{idp} - n_{par})] \times average\{(FF - FF_{sim})/esd_{FF}\}^2$ where n_{par} = number of refined parameters and n_{idp} = number of independent data points = 2 (2.45 - 0.90 Å) (14.3 - 2.2 Å^{-1}) / π = 11.9. [h] The uncertainty range is that over which the parameter can be fixed (while refining other parameters) without increasing ε_v^2 by more than 1.0 above the minimized value. The allowed positive and negative deviations from the refined value were similar (within 10%); the average of these deviations is reported as the ± quantity.

are identical within the estimated standard deviations or uncertainty ranges. The EXAFS analysis does have some minor differences in the secondary coordination spheres between the monomeric $[Co(III)\mathbf{1}(dmap)_2]^+$ and P-**1**$[Co(III)(dmap)_2]^+$. Steric crowding of the dmap and/or salen ligands confined within the immobilized sites might cause these slight differences. While confinement within the porous host may cause structural distortions, they appear to be minor based on the relatively small changes in the EXAFS data. Taken together the XANES and EXAFS data provide strong evidence that the cobalt coordination environment is changed only slightly during the polymerization of $[Co(III)\mathbf{1}(dmap)_2]^+$ and $[Co(III)\mathbf{2}(1\text{-MeIm})]^+$.

XANES and EXAFS Results for the Co(II) Polymers

We have also used XAS to probe the structure of the cobalt complexes in P-**1**[Co(II)] and P-**2**[Co(II)], which were formed by chemical modification of the immobilized sites after polymerization. Fig. 7 also contains the XANES spectra for P-**1**[Co(II)] and P-**2**[Co(II)], which shows that the K-edge energies for the two Co(II)-containing polymer are similar at 7719.49 (P-**1**[Co(II)]) and 7718.96 eV (P-**2**[Co(II)]). The shift to lower energy by ~3 eV in these samples compared to spectra for the Co(III) systems is consistent with more electron-rich Co(II) centres. For P-**1**[Co(II)], there is a significant shoulder at 7715.3 eV, which we have assigned as the 1s→4p transition. The prominence of this feature relative to the 1s→3d transition, which is found at 7709.9 eV, is indicative of a square planar geometry—an assignment that is based on XANES studies for a variety of nickel coordination compounds[22].

The analysis of the EXAFS of the Co(II) polymers shows the expected changes in coordination number for the immobilized cobalt complexes: four-coordinate complexes for P-**1**[Co(II)] and five-coordinate complexes for P-**2**[Co(II)]. All our analyses of the first and second spheres agree with these decreases in coordination number compared to those of the initially prepared polymers, P-**1**$[Co(III)(dmap)_2]$ and P-**2**[Co(III)(1-MeIm)]. The refined average bond lengths in P-**1**[Co(II)] are 1.86 Å and those in P-**2**[Co(II)] are 1.96 Å— these distances are similar to those in square planar and square pyramidal Co(II) Schiff base complexes such as *meso*-(N,N'-cyclohexylene-bis(salicylideneiminato)cobalt(II) (average r(Co—X) = 1.866 Å)[23] and [Co(II)**4**(pyridine)] (**4**, *N,N'*-(2,3 butylene)bis (salicylideneiminate)) (average r(Co—X) = 1.937 Å)[24].

The structural results obtained from EXAFS studies on P-**2**[Co(II)] are particularly interesting. Previously reported studies[25] have found that monomeric, five-coordinate Co(II) complexes with similar pentadentate Schiff base ligands to **2** have *trigonal bipyramidal* coordination geometry. In contrast, our data clearly indicated that *square pyramidal* Co(II) complexes exist within the porous hosts in P-**2**[Co(II)]. Note that

ligand **2** in the template complex [Co(III)**2**(1-MeIm)]$^+$, which was used to form the immobilized sites in P-**2**[Co(III)(1-MeIm)], also adopts a square pyramidal coordination geometry about the Co(III) ion. Subsequent demetallation, hydrolysis, reformation of **2**, and Co(II) ion binding does not significantly alter the coordination properties of the immobilized ligands. Therefore, a square pyramidal coordination geometry is maintained around the immobilized Co(II) ions in P-**2**[Co(II)], as opposed to converting to a trigonal bipyramidal arrangement, which is observed in related monomeric Co(II) complexes. This is an important result because it provides evidence that the organic host regulates the site structure in order to retain the coordination environment of the template complex, even after the immobilized sites have undergone extensive chemical modification.

EPR Studies on P-1[Co(II)] and P-1·py[Co(II)][4c,d]

We have also used X-band EPR spectroscopy to investigate the structures of the immobilized Co(II) complexes in our porous materials. Frozen suspensions of P-**1**[Co(II)] at 77 K gave an axial EPR spectrum, which is consistent with a square planar coordination geometry and corroborates our XAS results (Fig. 8A). Greater than 80% of these Co(II) sites in P-**1**[Co(II)] bind pyridine (P-**1**[Co(II)py]) or dmap (P-**1**[Co(II)dmap]) to form materials with immobilized five-coordinate complexes. The binding of an exogenous ligand can be followed by EPR spectroscopy. For instance, treating a suspension of P-**1**[Co(II)] with 15 equivalents of pyridine forms P-**1**[Co(II)py], which causes a pronounced change from an axial EPR spectrum to one that is rhombic (Fig. 8b). These changes in EPR properties serve as a spectral indicator for the formation of five-coordinate complexes within the immobilized sites, consistent with pyridine binding to an axial coordination site on the Co(II) centres.

The EPR spectrum for suspensions of P-**1**·**py**[Co(II)] (Fig. 8C) are more complicated than those for P-**1**[Co(II)] and P-**1**[Co(II)py] and show that the immobilized sites have a mixture of square pyramidal (5-coordinate) and square planar (four-coordinate) Co(II) centres. The distribution of coordination geometries is dependant on the solvent in which the P-**1**·**py**[Co(II)] is suspended: for CH_3NO, the solvent used to grow the porous solid, fitting of the EPR spectrum reveals 60% of the immobilized sites have square pyramidal complexes, while 40% have square planar geometry. In contrast, the percentages changes to 30% five-coordinate sites when P-**1**·**py**[Co(II)] is suspended in cyclohexane or diethyl ether.

These results are consistent with an equilibrium of four- and five-coordinate Co(II) complexes in the immobilized sites of P-**1**·**py**[Co(II)], and agree with known solution equilibria for Co(II)salen complexes[26]. The observation of an equilibrium of complexes in P-**1**·**py**[Co(II)] suggests that the immobilized sites are more dynamic than originally postulated by others. While the endogenous pyridine and salen ligands are correctly positioned within the site, they may not be preorganized or rigidly held in place as functional groups

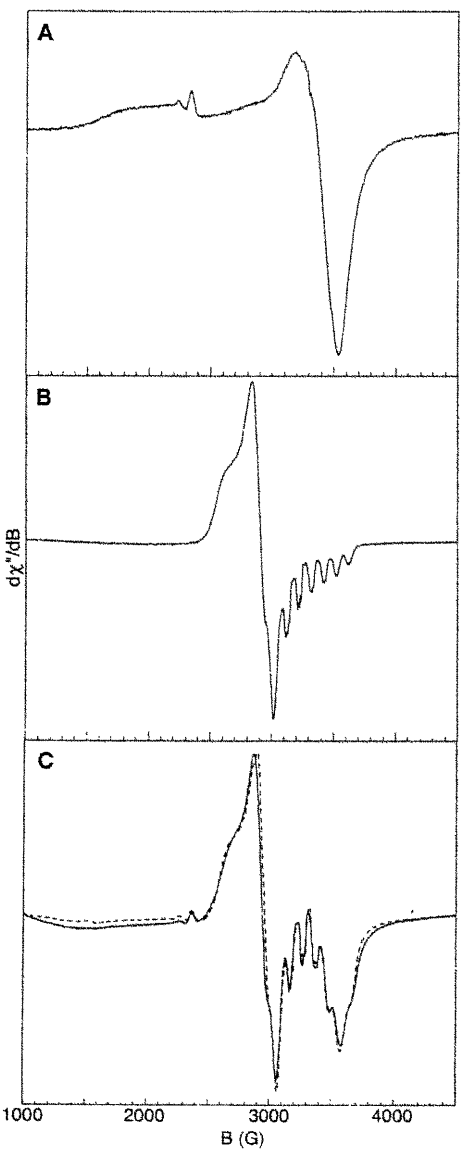

Fig. 8 X-band EPR spectra measured at 77 K for nitromethane suspensions of P-**1**[Co(II)] (A), P-**1**[Co(II)(py)] (B) and P-**1**·**py**[Co(II)] (C) suspended in CH_3NO_2. The spectral fits are indicated by broken-lines in panel **C**.

are in some molecular systems. We have proposed that this flexibility is a result of the three-point immobilization used to produce the cobalt sites. There is inherent flexibility because of the strylyoxy and vinyl linker groups used to attach the template to the polymethacrylate host. Because the binding of the axial pyridine ligand to the immobilized Co(II) centres should be weak, based on molecular systems studied in solution, a small amount of conformational flexibility between the pyridine and salen ligands within the sites would give rise to the observed distribution of four- and five-coordinate sites.

The changes in the percentage of four- and five-coordinate sites when P-**1**·**py**[Co(II)] is suspended in different solvents also has important ramifications. The highest degree of five-coordinate sites, which are the most organized structures, occurs when P-**1**·**py**[Co(II)] is suspended in CH_3NO_2, the solvent used during polymerization. A *solvent memory* effect is proposed, which influences the formation of the immobilized sites and, in turn, affects the Co(II) coordination geometry. During the copolymerization process it is reasonable to assume that the template complex is solvated, resulting in the actual template being a combination of a Co(III) complex and some number of CH_3NO_2 molecules. When P-**1**·**py**[Co(II)] is suspended in CH_3NO_2, the immobilized Co(II) sites can accommodate the CH_3NO_2 molecules and the greatest percentage of five-coordinates sites is observed. When other solvents not present at polymerization are used to suspend the polymer, they can interfere with the binding of the endogenous pyridine ligand, which leads to the observed lower percentage of 5-coordinate Co(II) sites.

Site Isolation: Dioxygen Binding to P-1[Co(II)dmap] and P-1[Co(II)py][4c,d]

P-**1**[Co(II)dmap] contains immobilized Co(salen)dmap complexes that should have the correct structure (i.e., square pyramidal coordination geometry) to readily bind dioxygen. The idea was confirmed by the EPR data shown in Fig. 9—exposure of P-**1**[Co(II)dmap], suspended in toluene, to dioxygen at room temperature produces a sample whose EPR spectrum is diagnostic for Co-superoxo sites. Spin concentration of the signal indicates that ~70% of the cobalt sites have dioxygen bound after 3 h—this value drops to 50% after 12 h. Nearly identical results were obtained for P-**1** [Co(II)py].

To show that the porous network polymer is stabilizing the Co-superoxo species in P-**1**[Co(II)dmap]

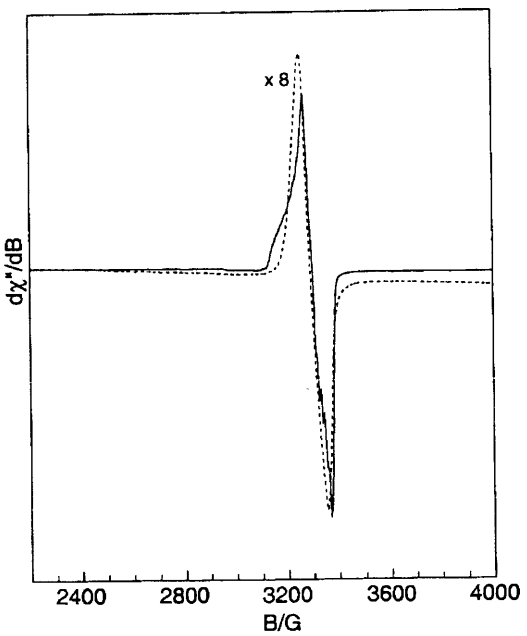

Fig. 9 X-band EPR spectra of P-**1**[Co(dmap)(O_2)] 1 hour after exposure to O_2 and collected at 77 K, (—) and 298 K, (----).

and P-**1**[Co(II)py], and preventing the decomposition to the Co(III)-(μ-peroxo)-Co(III) complex, O_2 was added to solutions of monomeric [Co(II)**1**(damp)] and [Co(II)**1**py] dissolved in 1:1 CH_2Cl_2-toluene at room temperature. After 3 h, the signal for Co-superoxo is almost completely gone when measured at 77 K and is not observable at room temperature. These results are corroborated by ^1H NMR studies that show the formation of the diamagnetic Co(III)-(μ-peroxo)-Co(III) dimer. In contrast, an EPR signal for P-**1**[Co(damp)O_2] is observable for over 12 d. These experiments are important because they clearly demonstrate the site isolation capabilities of the highly crosslinked porous network hosts. In P-**1**[Co(dmap)O_2] and P-**1**[Co(py)O_2], the polymethacrylate hosts stabilize reactive Co-superoxo species by preventing interactions with neighbouring Co-complexes.

Reversible Dioxygen Binding to P-1·py[Co(II)][4d]

Complete conversion to the Co—O_2 polymer P-**1**·**py**[Co—O_2] was achieved by exposing a suspension of P-**1**·**py**[Co(II)] in nitromethane to dioxygen for 2 min. The X-band EPR spectrum of this oxygenated sample is shown in Fig. 10A and clearly demonstrates the formation of Co—O_2 species within the immobilized sites[17,22,27]. The spin concentration of this signal showed that approximately 90% of the immobilized cobalt sites bound dioxygen. To our

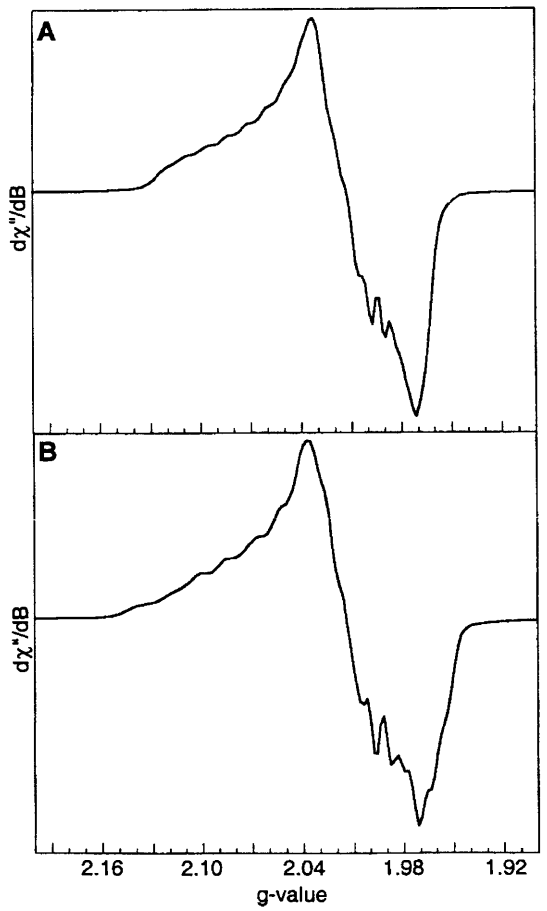

Fig. 10 X-band EPR spectra measured at 77 K for CH_3NO_2 (**A**) and cyclohexane (**B**) suspensions of P-**1**·**py**[Co—O_2]

knowledge, this is the largest value reported for immobilized Co(II) complexes within a porous host, including our systems (e.g, P-**1**[Co(dmap)O_2]) and those reported for similar complexes confined in zeolite cages[28]. For example, only 1% of the cobalt sites are oxygenated in zeolite NaY containing immobilized Co^{II}(salen)(py) complexes[29g].

Purging dioxygen through suspensions of P-**1**·**py**[Co(II)] in other solvents gave nearly identical EPR spectra for P-**1**·**py**[Co—O_2] as that obtained in CH_3NO_2, showing that the formation of the Co—O_2 sites is independent of suspending solvent. This is illustrated in Fig. 10B for P-**1**·**py**[Co—O_2] suspended in cyclohexane. Notice that all the EPR spectra of the P-**1**·**py**[Co—O_2] suspensions contain sharp, well-resolved signals, which indicates that all the immobilized Co—O_2 complexes have similar structures, with only minor heterogeneity at the metal centres. In addition, there is no evidence of signals associated with the four-coordinate Co(II) complexes in the spectra of P-**1**·**py**[Co—O_2]. This lack of a four-coordinate signal implies that the endogenous pyridine ligands in the immobilized sites are positioned within bonding distance of the cobalt centres. Based on the known coordination of Co(II)salen complexes (Scheme 2), this positioning is necessary to form the immobilized Co**1**(py)(O_2) complexes that yield the observed EPR spectra. To test this idea, we have examined the dioxygen binding properties of P-**1**[Co(II)], which has limited dioxygen binding with < 5% of the sites forming the Co—O_2 adducts. This limited dioxygen affinity for P-**1**[Co(II)] is illustrated in Fig. 11 for a suspension of polymer in cyclohexane.

X-band EPR was also used to monitor the reversible binding of dioxygen to P-**1**·**py**[Co(II)] (Fig. 12). Removal of dioxygen from P-**1**·**py**[Co—O_2] is accomplished by purging the system with N_2 for 3 min. Rebinding of O_2 to P-**1**·**py**[Co(II)] produces identical EPR spectra to that obtained initially for P-**1**·**py**[Co—O_2]. Spin concentration studies of the spectra associated with P-**1**·**py**[Co—O_2] show no decomposition of the cobalt binding sites during oxygenation.

Conclusion

Our results show that using a "molecules to materials" method, new *functional* porous materials can be designed and prepared. The use of inert metal complexes as templates, in conjunction with copolymerization methods, has allowed us to accurately place ligand donors within immobilized sites that are dispersed throughout porous materials. This methodology provides a framework for manipulating the length scale of these immobilized metal ion sites—continued efforts are needed to determine how the disposition of functional ligands can be used to design new, large inorganic species.

Polymers made by template copolymerization methods often have structural heterogeneity in the immobilized sites. Spatial misplacement of the functional groups within the immobilized sites is one possible cause for this heterogeneity[a]. Studies on the properties of the Co(II) sites in P-**1**·**py**[Co^{II}] indicate that the 4- and 5-coordinate complexes present within the sites result from the conformational flexibility of ligands, as opposed to misplacement of the ligands. This flexibility is attributed to linkers used to attach the ligands to the polymer host—in particular, the non-rigidity and low number of vinyl and

[a]Heterogeneous site structure is observed with templates formed from either covalent or non-covalent interactions; however, heterogeneity is more prevalent in systems that use non-covalent templates.

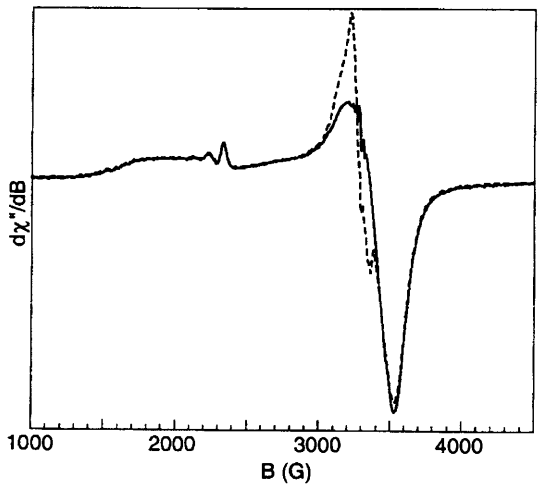

Fig. 11 X-band EPR spectra measured at 77 K for a cyclohexane suspension of P-**1**[Co(II)] under an atmosphere of Ar (—) and O_2 (-----).

strylyoxy linkers. It is likely that similar types of conformational flexibility are present in other polymers made by this method. In fact, to our knowledge, the majority of templated copolymers use only one linker to connect each functional group to the rigid polymer host. This results in rotamers being present in the immobilized sites that could contribute to dysfunction. However, flexibility within a site does not necessarily lead to non-functional materials. For instance, the conformational flexibility of ligands in the immobilized sites of P-**1**·**py**[Co^{II}] does not hinder its functional properties, as shown by 90% of the sites being able to reversibly bind dioxygen. In fact, conformational flexibility at the immobilized metal sites, as observed in P-**1**·**py**[Co^{II}], can be advantageous if applied correctly, such as in catalyst development[7c,29]. In these applications, having flexible active site models the behaviour of metal complexes in solution. This offers the intriguing prospect of developing solid materials whose immobilized metal complexes have properties akin to

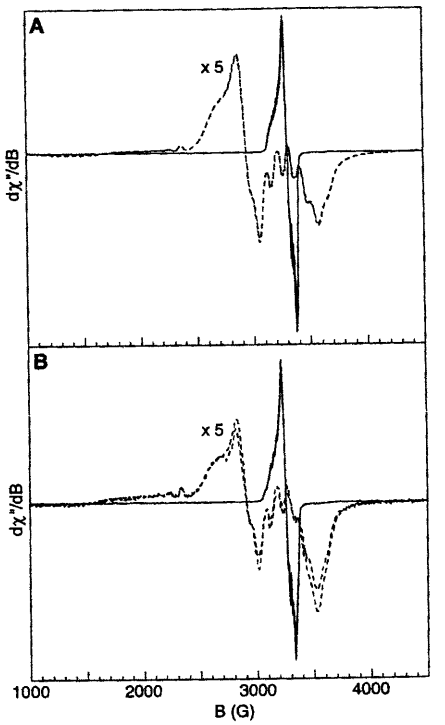

Fig. 12 X-band EPR spectra measured at 77 K for CH_3NO_2 (**A**) and cyclohexane (**B**) suspensions of P-**1**·**py**[Co(II)] (----) showing reversible dioxygen binding to form P-**1**·**py**[Co—O_2] (----). Two cycles are presented

analogs dissolved in solution. If achieved, the benefits of these types of systems are numerous.

Acknowledgements

The author is indebted to the many wonderful coworkers who have made this research possible: John Krebs, Anjal Sharma, Vivek Joshi, Karen Padden, Jeremy Koch, Leilani Welbes and Rob Scarrow. Financial support of this work was provided by ONR-DEPSCoR and NIH. The Bruker EMX-EPR spectrometer was purchased with funds obtained from the ONR-DURIP program.

References

1 J M Lehn *Angew Chem Int Ed Engl* **27** (1988) 90

2 O M Yaghi, H Li, C Davis, D Richardson and T L Groy *Acc Chem Res* **31** (1998) 474

3 J J Sokol, A G Hee and J R Long *J Am Chem Soc* **124** (2002) 7656

4 (a) J F Krebs and A S Borovik *J Am Chem Soc* **117** (1995) 10593; (b) J F Krebs and A S Borovik *Molecular and Ionic Recognition with Imprinted Polymers* (Eds. R A Bartsch and M Maeda) American Chemical Society Washington D C (1998) 159; (c) J F Krebs and A S Borovik *Chem Comm* (1998) 553; (d) A C Sharma and A S Borovik *J Am Chem Soc* **122** (2000) 8946; (e) K M Padden, J F Krebs, C E MacBeth, R C Scarrow and A S Borovik *J Am Chem Soc* **123** (2001) 1072; (f) A Sharma, V Joshi and A S Borovik *J Poly Chem Part A Poly Chem* **39** (2001) 888; (g) K M Padden, J F Krebs, K T Trafford, G P A Yap, A H Rheingold, A S Borovik and R C Scarrow *Chem Mat* **13** (2001) 4305

5 (a) M F Perutz, G Fermi, B Luisi, B Shaanan and R C Liddington *Acc Chem Res* **20** (1987) 309; (b) B A Springer, S G Sligar, J S Olsen and G N Philips Jr *Chem Rev* **94** (1994) 699; (c) B Shaanan *Nature* **296** (1982) 683; (d) P J Condon and W E Royer Jr *J Biol Chem* **269** (1994) 25259; (c) S E V Philips and B P Schoenborn *Nature* **292** (1981) 81

6 S Ozaki, M P Roach, T Matsui and Y Watanabe *Acc Chem Res* **34** (2004) 818

7 (a) J H Dawson *Science* **240** (1988) 433; (b) P R Ortiz de Montellano *Acc Chem Res* **20** (1987) 289; (c) P Ortiz de Montellano (Ed.) *Cytochrome P450* Plenum New York (1986)

8 J C Boyington, B J Gaffney and L M Amzel *Science* **260** (1993) 1482

9 (a) G Wulff *Angew Chem Int Ed Engl* **34** (1995) 1812 ; (b) K Mosbach and O Ramstrom *Biotechnology* **14** (1996) 163; (c) M E Davis, A Katz and W R Ahmad *Chem Mater* **8** (1996) 1820; (d) D Spivak and K J Shea *J Org Chem* **64** (1999) 4627

10 (a) P K Dhal and F H Arnold *Macromolecules* **25** (1992) 7051; (b) B B De, B B Lohray, S Sivaram and P K Dhal *Macromolecules* **27** (1994) 1291; (c) B P Santora, A O Larsen and Gagné *Organometallics* **17** (1998) 3138; (d) H Chen, M M Olmstead, R L Albright, J Devenyi and R H Fish *Angew Chem Int Ed Engl* **36** (1997) 642; (e) G D Saunders, S P Foxon, P H Walton, M J Joyce and S N Port *Chem Commun* (2000) 273; (f) N M Brunkan and M R Gagné *J Am Chem Soc* **122** (2000) 6217

11 G Barany and R B Merrifield, *Solid-Phase Peptide Synthesis The Peptides* (Eds. E Gross and J Meienhofer) Academic Press New York **2** (1980) 1

12 (a) F R Hartley *Supported Metal Catalysts* (Ed. D Riedel) Dordrecht Holland (1985); (b) *Syntheses and Separations Using Functionalized Polymers* (Eds. DC Sherrington and P Hodge) Wiley New York (1988); (c) B C Gates *Catalytic Chemistry* Wiley New York (1992); (d) *Chiral Reactions Heterogeneous* (Eds. G Jannes and V Dubois) Plenum Press Brussels (1990)

13 (a) J H Wang *Acc Chem Res* **3** (1970) 90; (b) J P Collman and C A Reed *J Am Chem Soc* **95** (1973) 2048; (c) O Leal, D L Anderson, R G Bowman, F Basolo and R L Burwell Jr *J Am Chem Soc* **97** (1975) 5125; (d) R S Drago, J Gaul, A Zombeck and D K Straub *J Am Chem Soc* **102** (1980) 1033

14 (a) H Han and K D Janda *J Am Chem Soc* **118** (1996) 7632; (b) A Petri, D Pini, S Rapaccini and P Salvandori *Chirality* **7** (1995) 580

15 (a) R Grubbs, C P Lau, R Cukier and C Brubaker Jr *J Am Chem Soc* **99** (1977) 4517; (b) J H Golden, H Deng, F J DiSalvo, J M J Fréchet and P M Thompson *Science* **268** (1995) 1463

16 (a) W F Maier, J A Martens, S Klein, J Heilmann, R Parton, K Vercruysse and P A Jacobs *Angew Chem Int Ed Engl* **35** (1996) 180; (b) M J Sabater, A Corma, A Domenech, V Fornés and H Garcia *Chem Commun* (1997) 1285; (c) R F Howe and J H Lunsford *J Am Chem Soc* **97** (1975) 5156; (d) N Herron *Inorg Chem* **25** (1986) 4714

17 I F J Vankelcom. D Tas, R F Parton, V Van de Vyver and P A Jacobs *Angew Chem Int Ed Engl* **35** (1996) 1346

18 K T Wan and M E Davis *Nature* **370** (1994) 449

19 (a) K J Shea and D Y Sasaki *J Am Chem Soc* **113** (1991) 4109; (b) A Katz and M E Davis *Nature* **403** (2000) 286

20 M Cesarotti, A Gullotti, A Pasini and R Ugo *J Chem Soc Dalton Trans* (1977) 757

21 (a) M J Carter, P P Rillema and F Basolo *J Am Chem Soc* **96** (1974) 392; (b) I K Meier, R M Pearlstein, D Ramprasad and G P Pez *Inorg Chem* **36** (1997) 1707

22 G J Colpas, M J Maroney, C Bagyinka, M Kumar, W S Willis, S L Suib, N Baidya and P K Mascharak *Inorg Chem* **30** (1991) 920

23 N Bresciani, M Calligaris, G Nardin and L Randaccio *J Chem Soc Dalton Trans* (1974) 1606

24 N Bresciani, M Calligaris, G Nardin and L Randaccio *J Chem Soc Dalton Trans* (1974) 498

25 (a) R Cini and P Orioli *Inorg Chim Acta* **63** (1982) 243; (b) R Boca, H Elias, W Haase, M Huber, R Klement, L Müller, H Paulus, I Svoboda and M Valko *Inorg Chim Acta* **278** (1998) 127

26 F A Walker *J Am Chem Soc* **95** (1973) 1150

27 D Getz, E Melemud, B C Silver and Z Dori *J Am Chem Soc* **97** (1975) 3846

28 (a) R F Howe and J H Lunsford *J Phy Chem* **75** (1975) 1836; (b) N Herron *Inorg Chem* (1986) 4714; (c) R F Howe and J H Lunsford *J Am Chem Soc* **116** (1994) 4746 (d) P K Dutta and C Bowers *Langmuir* **7** (1991) 937; (e) R S Drago, J Gaul, A Zombeck and D K Straub *J Am Chem Soc* **102** (1980) 1033; (f) R J Taylor, R S Drago and J P Hage *Inorg Chem* **31** (1992) 253; (g) D E De Vos, E J P Feijen, R A Schoonheydt and P A Jacobs *J Am Chem Soc* **116** (1994) 4746

29 (a) D E Koshland, Jr *Angew Chem Int Ed Engl* **33** (1993) 2375; (b) M Gerstein, A M Lesk and C Chothia, *Biochemistry* **33** (1994) 6739